https://doi.org/10.5194/egusphere-2025-3157
Preprint. Discussion started: 10 October 2025

Spatial-scale dependence of aerosol indirect effects over land in eastern China: A comparative analysis

Yuqin Liu[1,2], Tao Lin[1,2], Jiahua Zhang[3], Fu Wang[4], Meixia Lin[1,2], Yuan Chen[1,2], Yiyi Huang[1,2], Hongkai Geng[1,2], Xin Cao[1,2], Gerrit de Leeuw[5,6]

1 State Key Laboratory of Regional and Urban Ecology, Institute of Urban Environment, Chinese Academy of Sciences, Xiamen 361021, China
2 Fujian Key Laboratory of Digital Technology for Territorial Blank Analysis and Simulation, Fuzhou 350108, China
3 Key Laboratory of Digital Earth Sciences, The Aerospace Information Research Institute, Chinese Academy of Sciences, Beijing 100094, China
4 CMA Earth System Modeling and Prediction Centre (CEMC), Beijing 100081, China
5 Royal Netherlands Meteorological Institute (KNMI), R&D Satellite Observations, 3730AE De Bilt, The Netherlands
6 State Key Laboratory of Remote Sensing and Digital Earth & Key Laboratory of Satellite Remote Sensing of Ministry of Ecology and Environment, Aerospace Information Research Institute, Chinese Academy of Sciences, Beijing 100101, China

Correspondence to: Tao Lin (tlin@iue.ac.cn); Gerrit de Leeuw (gerrit.de.leeuw@knmi.nl, ORCID: 0000-0002-1649-6333)

Abstract

Regulatory effects of liquid water path (LWP) on cloud droplet effective radius (CER) and the interaction between aerosol optical depth (AOD) and cloud properties were systematically investigated. MODIS and CALIOP observed aerosols and clouds over eastern China in two periods: 2008–2014 (period 1) and 2015–2022 (period 2). The results show two distinct regimes of the variation of CER with LWP: a rapid growth regime (LWP < 55/50 g/m²) and a decreasing regime (LWP = 55-135/50-100 g/m²) (thresholds vary by period). The sensitivity of CER to AOD (S_{CER}) shows a negative correlation, and the S_{CER} in the LWP regime 2 shows larger than that in LWP regime 1. Here, the spatial scale is described by buffer size and study area. Overall, $|S_{CER}|$ decreases with increasing spatial scale. The optimal buffer sizes show notable variations in the range from 6°×6° to 10°×10°: increasing as study areas increase in period 2, but decreasing in period 1 for LWP regime 2. Compared with period 1, $|S_{CER}|$ in period 2 exhibits significantly decreases, reflecting the weaker of aerosol-cloud interactions for declining aerosol concentrations. Additionally, the sensitivity of N_d (cloud droplet number concentration) to AOD (S_{Nd}) shows a positive

https://doi.org/10.5194/egusphere-2025-3157
Preprint. Discussion started: 10 October 2025

correlation, with S_{Nd} decreases as spatial scale increases. The optimal buffer sizes show larger in the 8°×8° and 10°×10° regions than that in the 4°×4° and 6°×6° areas. This study reveals the scale-dependence of aerosol-cloud interactions.

Keywords: Aerosol, Cloud, Liquid water path, Scale effect, Satellite, Eastern China

1 Introduction

Aerosol particles, depending on their chemical composition and size, can serve as cloud condensation nuclei (CCN) in liquid clouds or as ice nucleating particles (INP) in ice clouds. When CCN are activated, they can alter the microphysical properties of clouds and affect precipitation, indirectly impacting the Earth's radiative budget through aerosol-cloud interactions (aci) (Tao et al., 2012; Fan et al., 2016; Rosenfeld et al., 2019; Rao and Dey, 2020; Bellouin et al., 2020). An increase in CCN concentrations results in a larger number of cloud droplets (N_d), and if the cloud liquid water path (LWP) remains constant, it leads to a reduction in the cloud droplet effective radius (CER). The reduced CER leads to an increased reflection of solar radiation, i.e. a higher cloud albedo, and enhances radiative forcing due to aerosol-cloud interaction (RFaci). The impact of increasing aerosol particle numbers on cloud properties, while maintaining a constant LWP, is commonly known as the "Twomey" effect (Twomey, 1977; Feingold, et al., 2001; Matheson et al., 2005; Koren et al., 2005; Meskhidze and Nenes, 2010; Costantino et al., 2010; 2013). Another aspect of RFaci involves quick adjustments, which could also cause changes in other cloud characteristics due to the rise in N_d and the decrease of CER. For example, this may lead to a reduction in precipitation efficiency, causing an increase in the LWP and cloud cover. As a result, the reflection of solar radiation is intensified (Albrecht, 1989). These two effects of aci are often categorized as the cloud albedo effect and the cloud lifetime effect (Quaas et al., 2008).

Extensive research on the impact of aerosols on the microphysical properties of clouds has been conducted utilizing satellite observations, aircraft measurements, ground-based monitoring, and numerical simulations. Among these, satellite-based instruments have become a vital observational tool for studying aerosol-cloud interactions due to their wide spatial coverage and high spatiotemporal resolution. However, optical satellite sensors such as the Moderate Resolution Imaging Spectroradiometer (MODIS) cannot effectively penetrate cloud layers, making it difficult to directly retrieve the optical properties of aerosols underneath clouds. Currently, aerosol data are mainly obtained in cloud-free conditions as determined using cloud detection methods. This limitation results in

https://doi.org/10.5194/egusphere-2025-3157
Preprint. Discussion started: 10 October 2025

significant spatial mismatches between aerosol and cloud properties, often requiring satellite data to be aggregated over large-scale grids for statistical analysis to determine relationships between aerosol and cloud parameters. The discrepancy between this large-scale analysis and the actual process scale frequently leads to biases in quantifying aerosol indirect effects, thereby significantly increasing the uncertainty in radiative forcing estimates (Lebsock et al., 2013; Altaratz et al., 2014; Ma et al., 2015; Possner et al., 2016; Bender et al., 2018).

In recent years, studies based on multi-source satellite data or multi-instrument joint observations have demonstrated that aerosol particles significantly influence cloud microphysical properties (Saponaro et al., 2017; Liu et al., 2018; Pandey et al., 2020). Numerous studies have validated the existence of the Twomey effect (Jones et al., 2009; Christensen et al., 2016; Jia et al., 2019). However, some studies have reported findings contradicting the Twomey effect, particularly over land, where an increase in AOD results in an increase in CER (Feingold et al., 2001; Yuan et al., 2008; Grandey and Stier, 2010; Tang et al., 2014; Wang et al., 2015; Ma et al., 2018; Jia et al., 2019; Liu et al., 2020). These inconsistent findings highlight the complexity and regional variability of aci mechanisms, and further in-depth research is needed to reveal the underlying processes.

Currently, researchers usually use grid methods (such as 1 °× 1 °, 2 °× 2 °, etc.) to study the aerosol indirect effects in large areas (Bréon, 2002; Kaufman et al., 2005; Bulgin et al., 2008; Quaas et al., 2008). For instance, Grandey and Stier (2010) estimated the relationship between aerosols and CER on a global scale (60°N~60°S) using multiple spatial resolutions (1°×1°, 4°×4°, 8°×8°, 15°×15°, and 60°×60°). They found that the aerosol indirect effect generally exhibited positive values over land and negative values over oceans. Additionally, the study highlighted that, when using grids larger than 4°×4° to investigate the relationship between aerosols and CER, significant errors could be introduced in calculating the aerosol indirect effect index due to the spatial variability of aerosol and cloud parameters.

For studies focusing on smaller regions, researchers often employ moving window or buffer zone methods. These approaches assume a uniform distribution of aerosol concentrations within the window or buffer zone with a certain area and construct spatially matched samples by averaging AOD and cloud parameters within the defined area. For example, Yuan et al. (2008) used a 100 km × 100 km moving window to calculate the mean values of aerosol and cloud properties, investigating the relationship between aerosols and CER across seven global regions. Their results indicated that only two of these

https://doi.org/10.5194/egusphere-2025-3157
Preprint. Discussion started: 10 October 2025

regions exhibited a positive correlation between CER and AOD. Similarly, Jones et al. (2009) utilized multi-source remote sensing data and applied a point spread function to compute aerosol and cloud properties within a 20 km range. Their study examined the influence of aerosol types, cloud conditions, and atmospheric factors on aerosol indirect effects across six different oceanic regions globally. In addition, significant progress has been made in research based on Cloud-Aerosol Lidar with Orthogonal Polarization (CALIOP) data. Costantino et al. (2010) investigated the relationship between aerosols and CER in stratocumulus clouds over the coastal regions of Namibia and Angola by calculating aerosol and CER within a 150 km buffer zone around CALIOP samples. Their study particularly focused on scenarios where aerosols and cloud layers were separated. Costantino et al. (2013) further analyzed the statistical relationship between aerosol concentrations and cloud physical parameters by examining aerosol and cloud properties within a 20 km buffer zone around CALIOP samples, integrating vertical profile data of aerosols and clouds. Wang et al. (2015) revealed an inverse "Twomey" effect between aerosols and CER in eastern China by analyzing aerosol and CER within a 50 km buffer zone around CALIOP samples. Similarly, Liu et al. (2017) systematically examined the response mechanisms of warm cloud macro- and microphysical parameters to increasing AOD in the Yangtze River Delta region, also using CALIOP samples within a 50 km buffer zone. More recently, Liu et al. (2024) quantified the relative importance of aerosols, meteorological parameters and their interactions on cloud properties in the eastern coastal and inland regions of China, utilizing MODIS 1°×1° aerosol and cloud product data. These studies have provided critical scientific insights into aci at regional scales.

However, the properties and interaction processes of aerosols and clouds exhibit significant spatial heterogeneity and scale dependency (McComiskey et al., 2009; McComiskey and Feingold, 2012; Chen et al., 2015; Glotfelty et al., 2020). In previous studies, the definitions of window size and buffer size have often been subjective, inadvertently introducing uncertainties into the research on aci. Although studies have explored the relationship between aerosols and CER across different observational scales, these investigations have primarily focused on larger spatial scales, leaving a gap in sensitivity analysis of aerosol indirect effects at smaller regional scales. Therefore, utilizing multi-source remote sensing data to explore whether and how the aerosol indirect effect depends on observational spatial scales in eastern China is of great significance for developing parameterization schemes that align with the regional characteristics of aci.

https://doi.org/10.5194/egusphere-2025-3157
Preprint. Discussion started: 10 October 2025

Aerosol properties in China have significantly changed between 2008 and 2022 due to economic development and the implementation of emission reduction policies. The AOD over China increased until 2007 to become among the highest worldwide and remained high between 2008 and 2014 with large interannual variations. The enforcement of emission reduction measures, in particular the implementation of the 2013-2017 Clean Air Action Plan, resulted in the decline of the AOD between 2014 and 2018 (de Leeuw et al., 2021; 2022; 2023) and a further decrease resulted in an AOD lower than that in 2000 (de Leeuw et al, 2023). Based on these observations, this study will conduct a comparative analysis of the sensitivity of cloud parameters (CER and N_d) to AOD variation based on data from two distinct periods: 2008-2014 (Period 1, high AOD) and 2015-2022 (Period 2, decreasing AOD). The main objective of this study is to investigate: (1) the effect of spatial scale on the sensitivity of CER to AOD (S_{CER}) across different time periods in the eastern region of China; and (2) the effect of spatial scale on the sensitivity of N_d to AOD (S_{Nd}) across different time periods in the eastern region of China. Through these two aspects of research, the study aims to reveal the sensitivity patterns of aerosol indirect effects to spatial scales, providing support for optimizing parameterization schemes and accurate assessment of regional aerosol effects.

2 Method

2.1 Study area

Eastern China (30°N-40°N, 112°E-122°E; Figure 1) has undergone remarkable economic expansion over the past three decades, which was accompanied by a substantial increase in AOD. Eastern China presents a unique atmospheric laboratory due to its complex aerosol composition - featuring both anthropogenic pollutants from industrial emissions and natural mineral dust transported from Central Asian deserts, particularly during the spring. The multitude of sources and the persistent nature of these aerosol particles, which can remain suspended for days to weeks and be transported over long distances in the absence of precipitation (Kim et al., 2007; Guo et al., 2013), makes eastern China an ideal study area for investigating aci. Our research leverages satellite observations to systematically evaluate the sensitivity of cloud properties (S_{CER} and S_{Nd}) to the AOD variation.

https://doi.org/10.5194/egusphere-2025-3157
Preprint. Discussion started: 10 October 2025

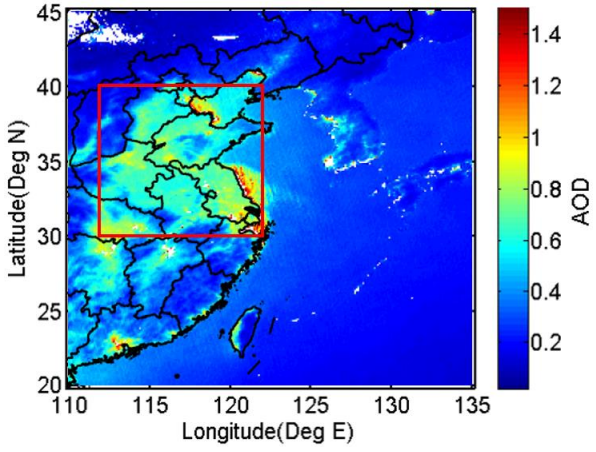

Figure 1. Map of annual averaged MODIS/AQUA level 2 AOD for all years during the period from 2008 to 2022. The red rectangle (30–40 N and 112–122 E) indicates the study area.

2.2 Data used

Data used in this study were acquired by the Moderate Resolution Imaging Spectroradiometer (MODIS) instrument aboard NASA's Aqua satellite, which features an extensive swath width of approximately 2300 km and comprehensive spectral coverage across multiple bands (King et al., 2003). The satellite's equator crossing time is 13:30 (LT), i.e. in the early afternoon, coinciding with optimal development conditions for continental warm cloud systems. For aerosol characterization, we utilized the MODIS Collection 6.1 aerosol product (MOD04), generated from cloud-screened pixels with a native resolution of 500 m at nadir and subsequently aggregated to 10 km grid cells (Remer et al., 2005; Levy et al., 2010). AOD retrieval over land uses radiances measured at the top of the atmosphere (TOA) at wavelengths of 0.47, 0.66, and 2.13 μm (Remer et al., 2005). In this study, AOD larger than 1.5 was excluded from further analysis to mitigate potential retrieval overestimation.

The cloud properties analysed in this study, including CDR, LWP, cloud optical thickness (COT), cloud top pressure (CTP), and cloud phase infrared (CPI) index, were derived from the MODIS Level 2 cloud product (MYD06) (King et al., 2003). The retrieval of these cloud characteristics utilizes six spectral channels spanning wavelengths from the visible to the near-infrared (0.66, 0.86, 1.24, 1.64, 2.12, and 3.75 μm) as described by King et al. (1997). Following the methodology of Platnick et al. (2017), CER and COT measurements at 3.7 μm are employed to estimate N_d through adiabatic approximation principles (Quaas et al., 2006). Previous investigations have demonstrated that implementing filters based

https://doi.org/10.5194/egusphere-2025-3157
Preprint. Discussion started: 10 October 2025

on cloud adiabaticity produces minimal effects on S_{Nd} estimates while significantly reducing the available dataset by up to 63% (Gryspeerdt et al., 2022). Therefore, such filtering procedures were not adopted in the current analysis. It should be noted that N_d calculations are initially performed at the native pixel resolution (approximately 1 km) prior to spatial aggregation, thereby avoiding potential biases associated with deriving N_d from nonlinear combinations of CER and COT at coarser resolutions (Feingold et al., 2022). To maintain data quality, the analysis incorporates several quality control measures: only single-phase liquid clouds (CPI = 1) with CTP exceeding 700 hPa and LWP below 200 g m^{-2} are considered, consistent with the typical atmospheric distribution of aerosols in the lower troposphere (Michibata et al., 2014). Pixels with CER values smaller than 4 μm or COT values smaller than 4 are excluded due to increased retrieval uncertainties (Sourdeval et al., 2016). Additionally, observations are restricted to solar zenith angles <65° and sensor zenith angles <41.4°. This constraint is intended to reduce the influence of well-documented biases, as elaborated in Grosvenor et al. (2018).

The Aqua satellite operates within the A-Train constellation alongside CALIPSO (Cloud-Aerosol Lidar and Infrared Pathfinder Satellite Observations) and other NASA Earth-observing platforms (Stephens et al., 2002). As a key instrument aboard CALIPSO, the Cloud-Aerosol Lidar with Orthogonal Polarization (CALIOP) represents the first space-based polarization-sensitive lidar system specifically designed for atmospheric profiling of aerosols and clouds (Winker et al., 2003). This advanced sensor features an exceptionally narrow ground footprint of 70 m diameter for each laser pulse. The vertical resolution of CALIOP's products varies with altitude: 30 m within 0-8.2 km, 60 m between 8.2-20.2 km, and 180 m from 20.2-30.1 km, while maintaining a consistent 5 km horizontal resolution along the track direction (Liu et al., 2009).

The coordinated A-Train configuration ensures near-simultaneous observations (within 1-2 minutes) between MODIS/Aqua and CALIOP/CALIPSO for identical atmospheric targets (Stephens et al., 2002). This temporal synchronization guarantees data consistency when extracting coincident measurements. For spatial compatibility, we resampled the higher-resolution MODIS cloud products (CDR, LWP, and N_d at 1 km native resolution) to match CALIOP's 5 km along-track scale, while directly utilizing the 5 km-resolution CTP and CPI parameters. In cases where CALIOP detected aerosol presence, we computed spatial averages of MODIS aerosol and cloud retrievals across multiple observation scales (detailed in Section 2.4) centred on CALIOP targets. This approach assumes reasonable homogeneity of

https://doi.org/10.5194/egusphere-2025-3157
Preprint. Discussion started: 10 October 2025

aerosol properties between adjacent clear and cloudy regions (Anderson et al., 2003; Quaas et al., 2008). Table 1 comprehensively documents the aerosol and cloud datasets employed in this investigation, including their respective parameters, resolutions, and sources.

Table 1. Aerosol and cloud products, parameters, horizonal resolutions, and their sources applied in the present study.

Product	Parameters	Horizontal resolution	Data source
Aerosol (MYD04 Level 2 Collection 5)	Latitude	10 km	MODIS
	Longitude	10 km	
	Scan_Start_Time	10 km	
	AOD at 550 nm	10 km	
Cloud (MYD06 Level 2 Collection 5)	Latitude	5 km	
	Longitude	5 km	
	Scan_Start_Time	5 km	
	CER at 3.7 um and 2.1 um	1 km	
	LWP at 3.7 um	1 km	
	COT at 3.7 um	1 km	
	Cloud multi-layer flag	1 km	
	Cloud_Phase_Infrared_Day	5 km	
	Cloud_TOP_Pressure_Day	5 km	
	Sensor_Zenith_Day	5 km	
	Solar_Zenith_Day	5 km	
Aerosol (05kmALay)	Latitude	5 km	CALIOP
	Longitude	5 km	
	Profile_Time	5 km	

2.3 Calculation of sensitivities

Variations in aerosol loading significantly influence cloud optical properties (such as COT) and microphysical parameters (such as CER). Under specific environmental conditions, aerosol particles can transform into CCN or INP, a process primarily determined by their chemical composition and ambient temperature. When these nuclei are activated, water vapor condenses on their surfaces to form cloud droplets or ice particles. As the concentration of aerosol particles increases, the number of CCN or INP may rise correspondingly, leading to an increase in the number of cloud droplets. Notably, under conditions where the liquid water content in clouds remains constant (i.e., LWP), the same amount of water vapor is distributed across more cloud droplets, resulting in a reduction in the size of individual droplets. Specifically, as aerosol concentration increases, the CER decreases, while cloud albedo increases. On the basis of findings of Kaufman and Fraser (1997), Feingold et al. (2001) pointed out that

https://doi.org/10.5194/egusphere-2025-3157
Preprint. Discussion started: 10 October 2025

the sensitivity of cloud microphysical properties (e.g., CER) to changes in the number concentration of aerosol particles (e.g., using AOD as a measure) can be described by the following formula:

$$S_{CER} = \frac{d \ln r_e}{d \ln \alpha}|_{LWP} \quad -0.33 < S < 0 \quad (1)$$

Where r_e represents the CER and α represents the AOD. Following Andreae (2009), AOD and CCN are correlated and AOD varies with CCN following a power law relationship. Eq. (1) describes the relative change of CER with the relative change of the AOD for constant LWP. It is noted that this formulation differs from that used in recent studies (e.g., Bellouin et al., 2020) where S is expressed in terms of N_d with no restriction in LWP. The sensitivity S of CER to AOD can be determined as the slope of a linear fit to a log-log plot of CER versus AOD.

Here, the variation in N_d with CCN is referred to as the susceptibility S_{Nd}. Following the method of Gryspeerdt et al. (2023), the sensitivity, S_{Nd}, of a cloud property, N_d, to α is defined here as

$$S_{Nd} = d \ln N_d / d \ln \alpha \quad 0 < S < 1 \quad (2)$$

Relations between CER and N_d and AOD are determined through Eq. 1 and Eq. 2 and correlation coefficients R. The significance of these relations is determined by using the student's t test, i.e. the results are statistically significant when the p value is smaller than 0.01, where p is defined as the probability of obtaining a result equal to or "more extreme" than what was actually observed.

2.4 Research design for scale effects analysis

This study was conducted at multiple spatial scales to examine the scale dependence of S_{CER} and S_{Nd} in delineating aci (Fig. 2). Here, the spatial scales are described by two parameters: study area size and buffer size. To this end, the study area was divided into four congruent square research areas all centered at the same geographical location (35°N, 117°E) over Eastern China. Hence, spatial extent varies from the whole study area as defined in Section 2.1 (30°N-40°N, 112°E-122°E) to successively smaller areas simulated by decreasing the study area in steps of 2° to 4°×4° as illustrated in Figure 2a. Buffer zones with sizes increasing from 10 to 300 km (10 km, 20 km, 30 km, 40 km, 50 km, 60 km, 70 km, 80 km, 90 km, 100 km, 120 km, 140 km, 150 km, 160 km, 180 km, 200 km, 250 km, and 300 km) were determined within the whole study area by using CALIOP data, i.e. data points where CALIOP detected the presence of aerosol and cloud fields. MODIS-retrieved cloud and aerosol data were averaged over a buffer area around each CALIOP data point with a radius varying from 10 km to 300 km. Thus, a dataset including

https://doi.org/10.5194/egusphere-2025-3157
Preprint. Discussion started: 10 October 2025

aerosol and cloud properties was constructed with different buffer sizes. The effect of buffer size on the sensitivity of CER and N_d to variations in AOD was determined in each study area varying from 4°×4° to 10°×10°.

The dataset was used to study the characteristics of aerosol indirect effects as function of buffer size and study area, for two different periods: one with a high aerosol content (2008-2014) and another one with a decreasing aerosol content (2015-2022). This approach enabled the determination of the optimal buffer size for aerosol indirect effects as function of the size of the study area, ultimately leading to the development of a parameterization scheme for aerosol indirect effects for observations with different spatial resolution and different sizes of the study area over eastern China.

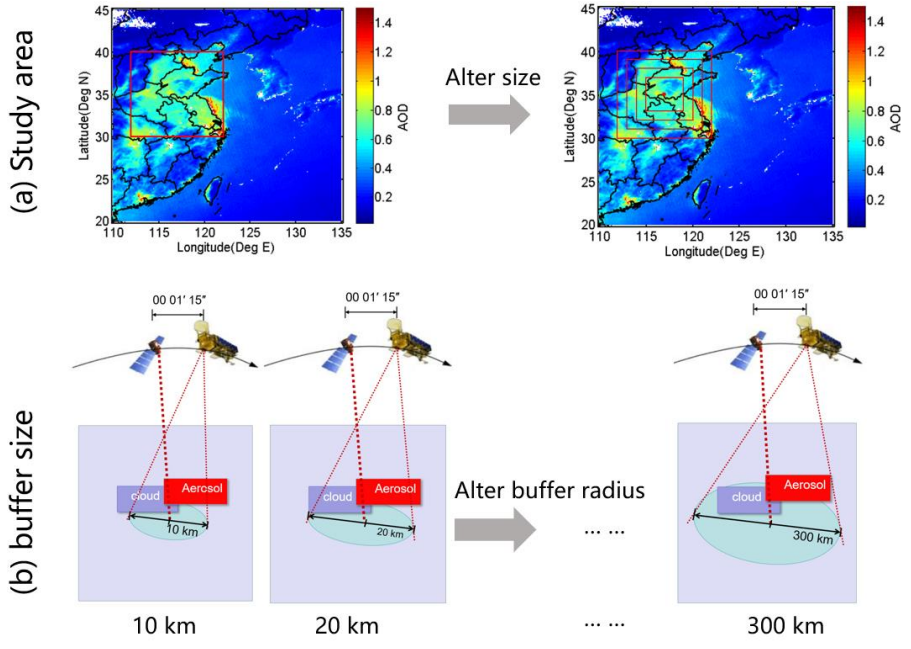

Figure 2. (a) Schematic diagram of study area and buffer size patterns applied in this study. (b) scheme of CALIPSO-MODIS coincidence methodology. When CALIPSO detects the presence of aerosol and cloud fields, we look for MODIS retrievals within a buffer size from the CALIPSO target. The temporal coincidence is insured by the coordinated satellite orbits.

3 Results

3.1 Spatial variations of aerosol and cloud parameters

Figure 3 illustrates the spatial distributions of AOD and cloud properties (CER and N_d) across the study

https://doi.org/10.5194/egusphere-2025-3157
Preprint. Discussion started: 10 October 2025

region, averaged for the periods 2008-2014 and 2015-2022. The AOD spatial patterns (Fig. 3a,d) show similar spatial distributions during both periods, but with notably reduced values during the latter. Pronounced spatial gradients in AOD are evident during both periods. The lowest AOD values occur over the mountainous regions of Shanxi province in the northwest, while elevated concentrations appear in the southeastern areas encompassing the Hebei and Shandong provinces. This geographical contrast arises from the mountain ranges that demarcate the heavily industrialized, densely populated North China Plain (NCP) in the east - characterized by substantial anthropogenic emissions - from the relatively pristine western regions. Under prevailing southeasterly wind conditions, these topographic barriers effectively block transport of atmospheric pollutants which accumulate along their windward slopes (Sundström et al., 2012). The concentration of heavy industries and power generation facilities in the NCP are primarily responsible for the observed high AOD concentrations., together with meteorological and geographical conditions. Additionally, lower AOD values appear in southern Anhui and central Shandong relative to the surrounding regions.

The CER spatial distributions (Fig. 3b,e) reveal distinct differences between the two periods. During 2008-2014, larger cloud droplets predominated in the northern sectors, particularly throughout Hebei and western Shandong. Notably, the spatial correspondence between AOD and CER maxima aligns with the anti-Twomey effect, suggesting that the high aerosol loading promoted cloud droplet growth rather than suppression - consistent with findings from Wang et al. (2014) and Liu et al. (2018). The 2015-2022 period shows markedly reduced CER values (typically <10 μm) with enhanced spatial homogeneity.

Similarly, N_d exhibits contrasting spatial patterns between the two periods (Fig. 3c,f). The earlier timeframe shows depressed N_d values in central regions surrounded by elevated concentrations peripherally. This pattern reverses during 2015-2022, with increases of N_d in the central area accompanied by overall reduction of the cloud droplet concentrations in the surrounding regions.

https://doi.org/10.5194/egusphere-2025-3157
Preprint. Discussion started: 10 October 2025

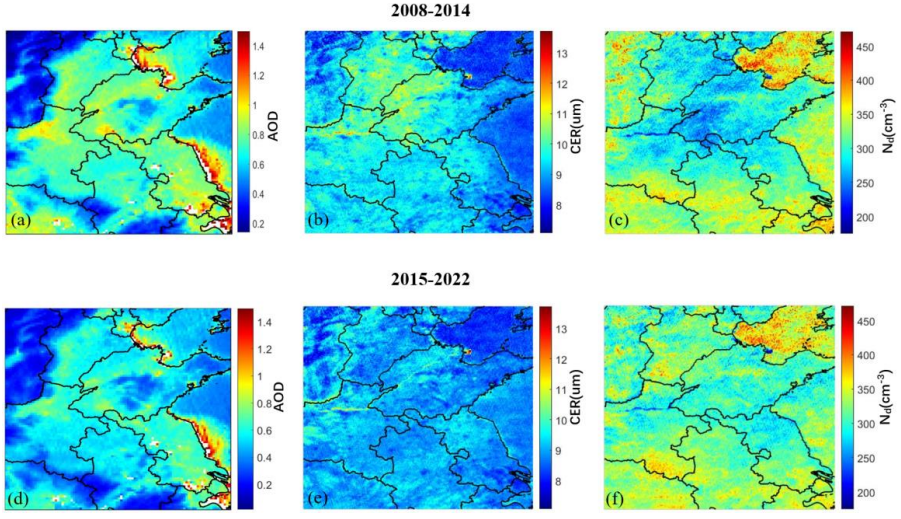

Figure 3. Spatial distributions of AOD (a, d), CER (b, e) and N_d (c, f), averaged over the years 2008-2014 (top row) and 2015-2022 (bottom row) over the study area.

3.2 Sensitivity of CER to AOD stratified by LWP

Before analyzing the influence of AOD on CER, the relationship between CER and LWP should be investigated. The values of the LWP were divided into 40 subsets with a width of 5 g/m^2, and then the average value of CER in each subset was calculated and plotted as function of LWP (Figure 4).

The variation of CER with LWP shows three regimes. For LWP smaller than 55 g/m^2 (period 1) or 50 g/m^2 (period 2), CER increased rapidly with the increase of LWP. This first regime is referred to as the rapid growth phase of CER. The second regime occurred when the LWP ranged from 55 g/m^2 to 135 g/m^2 (period 1) or 50-100 g/m^2 (period 2) and CER decreased with the increase of LWP. When LWP was greater than 135 g/m^2 (period 1) or 100 g/m^2 (period 2), CER increased with increasing LWP but at a much slower rate than during the first regime; the third regime is therefore referred to as the slow growth regime. These results show that CER is very sensitive to the changes in LWP, which is consistent with the study of Liu et al. (2021). To separate the effects of changing LWP on CER from those of changing AOD on CER, relations between CER and AOD were evaluated for constant LWP (McComiskey et al., 2012), for each of the three regimes mentioned above, by using double-logarithmic plots of AOD versus CER. The number of CER observations in the third regime is too small to achieve statistically meaningful results, therefore the sensitivity of CER to AOD was only analyzed for the rapid growth and decreasing

https://doi.org/10.5194/egusphere-2025-3157
Preprint. Discussion started: 10 October 2025

regimes.

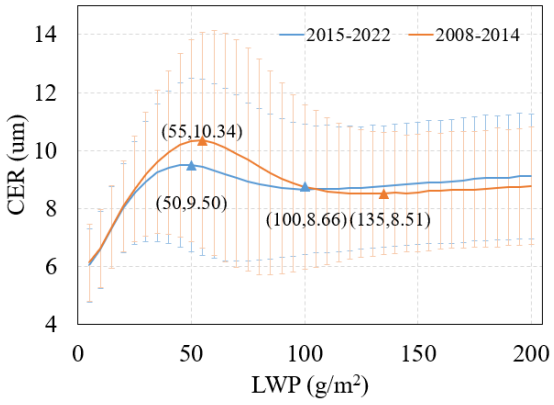

Figure 4. Variation of CER with LWP over the study area. Here all CER data were averaged in LWP bins, from 0 to 200 g/m^2 with a width of 5 g/m^2. The red line is for the data during 2008-2014 and the blue line is for the data during 2015-2022. The numbers in parentheses indicate the (LWP, CER) values for the inflection points between the regimes. The error bars (the vertical lines) denote the standard deviations, indicating the variability of CER around the average at each LWP value.

3.2.1 Rapid CER growth regime

For the first, rapid CER growth regime, the S_{CER} is negative (as shown in Figure 5). The increase of aerosols implies an increase in the number of CCN for which, at constant LWP, less water vapor is available per cloud droplet, causing the CER to become smaller, increasing the albedo of the cloud, and ultimately cooling the atmosphere. This indicates that, in regime 1, the interaction between AOD and CER in the target region is in agreement with the Twomey effect. The data in Figure 5a show that during Period 1, S_{CER} varies with buffer size and that the variations are different for different study areas. The value of $|S_{CER}|$ is smallest for the largest study area (10°×10°) and decreases with buffer size to a minimum for buffer size of 150 km and then increases. For the smallest study area (4°×4°), the sensitivity is much stronger negative and decreases as buffer size increases, especially for 50 km < buffer size < 100 km. For the 2 intermediate study areas, the sensitivities are initially similar (except for the smallest buffer size) and diverge for buffer size>100 km. The data show that the value of S_{CER} overall becomes smaller as study area increases. The correlation coefficients R (bottom of Figure 5 a) are similar for all four study areas at small buffer sizes, increase fast with buffer size to a maximum for a buffer size of about 50 km and then decrease and diverge. The largest decrease is observed for study area of 10°×10°. In this study,

https://doi.org/10.5194/egusphere-2025-3157
Preprint. Discussion started: 10 October 2025

the optimal scale for S_{CER} in a study area is defined as the buffer size with the highest correlation coefficient R between S_{CER} and AOD. The optimal scale for each study area is indicated in Figure 5 with a red solid square. A plot of the optimal scale versus the size of the study area in Figure 6 (curve LWP1-P1) shows that, as the study area size is increased from 6°×6° to 10°×10°, the optimal scale decreased from 100 km to 30 km.

As compared with period 1, in period 2 (Figure 5b) the value of the S_{CER} decreases as the buffer size increases. However, the scale sensitivity analysis for period 2 revealed two distinct characteristics different from period 1: (1) the four S_{CER} curves for different study areas are much closer than during period 1; (2) with the exception of the study area of 10°×10°, the values of S_{CER} curves for the other three study areas are significantly reduced (closer to zero), indicating a corresponding weakening of aerosol-cloud interaction intensity against the background of decreased aerosol concentrations. Particularly noteworthy is that during period 1, the R values for the study area of 10°×10° display a sharp attenuation trend when the buffer size exceeds 60 km, while in period 2 this happened for buffer size larger than 110 km and the R value curves for other study areas are markedly lower than for period 1, with their high-value ranges significantly expanded. Also for period 2, the R values for the study areas of 10°×10° and 8°×8° are very similar, in contrast to period 1 when only the R values for the study areas of 10°×10° decreases fast. In period 2, the R values for the study area of 4°×4° show a behavior similar to that for the study area of 10°×10° in period 1. Across different study areas, the optimal scale (Curve LWP1-P2) showed a behavior opposite to that during P1: as the study area size is increased from 6°×6° to 10°×10°, the optimal scale increased from 20 km to 80 km. It is noted that for a study area of 4°×4° the optical scale was 50 km in both periods P1 and P2. The estimates of S_{CER} and correlation coefficients R between CER and AOD, stratified by LWP and optimal buffer size, for study areas ranging from 4°×4° to 10°×10° during the 2008–2014 period are presented in A1.

3.2.2 Decreasing CER regime

During the second LWP regime (Figure 7), the AOD and CER were also negatively correlated (S_{CER}<0) during both periods, but the values of S_{CER} vary stronger with the size of study area: for the largest study area of 10°×10° the value of S_{CER} decrease with increasing buffer size to close to zero for a buffer size of about 150 m and reach a small positive value before it slowly decreases to below zero for a buffer size

https://doi.org/10.5194/egusphere-2025-3157
Preprint. Discussion started: 10 October 2025

of 220 m. For the three smaller study areas, the S_{CER} values were all negative and overall decreased with increasing buffer size. Through the sensitivity of S_{CER} to buffer size across varying study areas during period 1, the value of S_{CER} for a given buffer size becomes smaller with increasing study area size. Additionally, across all study areas, S_{CER} initially decreases with the increase of the buffer size, then increases, and gradually stabilizes thereafter. The data in Figure 6 (Curve LWP2-P1), show that, the optimal size varies between 30 km and 60 km with no clear dependence on the size of the study area.

Compared with the period 1, the S_{CER} in period 2 (Figure 7b) also decreased overall with increasing buffer size, and at the same buffer size, S_{CER} decreased (less negative) as study area increased. However, the scale sensitivity analysis for period 2 revealed two distinct characteristics: (1) the four curves for different study areas are closer than during period 1; (2) the S_{CER} for the study area of 10°×10° was overall smaller (more negative), while the values of the S_{CER} curves for the study areas of 4°×4° and 6°×6° were significantly reduced and that for the study area of 8°×8° was slightly reduced. The reduction may be attributed to weakened cloud-aerosol interactions resulting from decreased regional aerosol concentrations. The variation of the optimal scale (Curve LWP2-P2) with the size of the study area is similar to that during P2 in the rapid growth LWP regime: as the study area size is increased from 6°×6° to 10°×10°, the optimal scale increased from 60 km to 100 km. The estimates of S_{CER} and correlation coefficients R between CER and AOD, stratified by LWP and optimal buffer size, for study areas ranging from 4°×4° to 10°×10° during the 2015–2022 period are presented in A1.

Through comparative analysis of S_{CER} data distribution across different LWP regimes under different aerosol conditions (i.e. high AOD and decreasing AOD), we found that the S_{CER} in the second LWP regime is significantly larger than that in first LWP regime except for the study area of 10°×10° for buffer size >100 m, where S_{CER} curves corresponding to different study areas show greater dispersion.

https://doi.org/10.5194/egusphere-2025-3157
Preprint. Discussion started: 10 October 2025

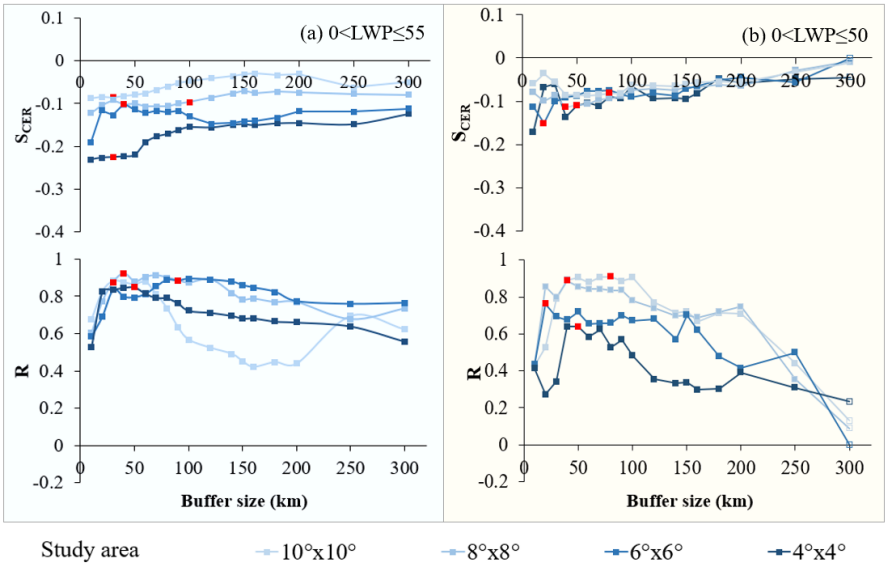

Figure 5. Variation of S_{CER} (top) and correlation coefficient R (bottom) with buffer size for different study areas (see legend below the figures) for (a) the LWP regime with 0<LWP≤55 g/m² over the years of 2008-2014 and (b) the LWP regime with 0<LWP≤50 g/m² over the years of 2015-2022. Solid squares indicate that the results are significant at the 0.01 level and hollow squares indicate that the results are not statistically significant. The red solid squares indicate the optimal buffer sizes for each study area, as shown in the Supplement Table 1.

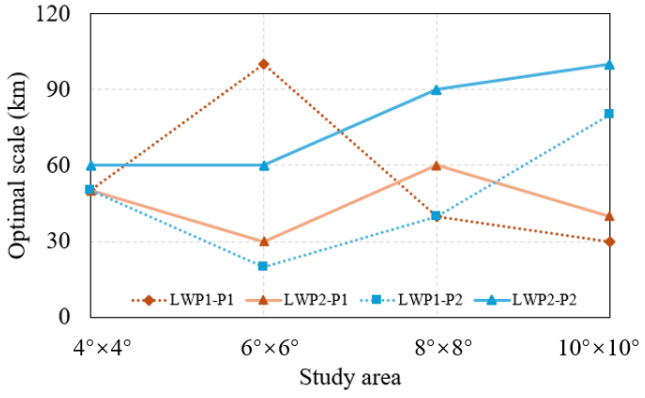

Figure 6. Relationship between optimal scale for S_{CER} and the size of the study area. Here LWP1-P1 and LWP2-P1 indicate the optimal scale in period 2008-2014 for the LWP regime1 and that for the LWP regime 2, respectively. LWP1-P2 and LWP2-P2 indicate the optimal scale in period 2015-2022 for the LWP regime1 and that for the LWP regime 2, respectively.

https://doi.org/10.5194/egusphere-2025-3157
Preprint. Discussion started: 10 October 2025

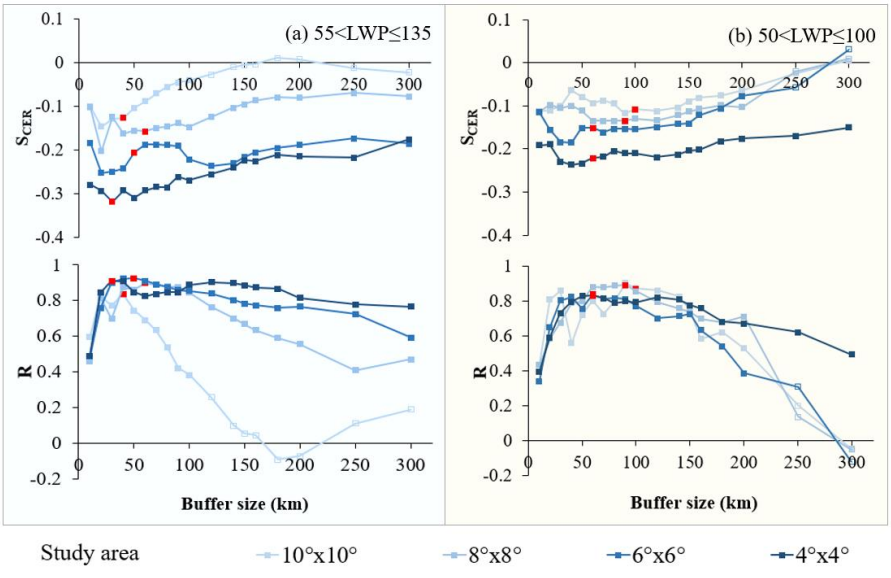

Figure 7. Variation of S_{CER} (top) and correlation coefficient R (bottom) with buffer size for different study areas (see legend below the figures) for (a) the LWP regime with 55<LWP≤135 g/m² over the years of 2008-2014 and (b) the LWP regime with 50<LWP≤100 g/m² over the years of 2015-2022. The solid square indicates that the results are significant at the 0.01 level and the hollow square indicates that the results are not statistically significant. The red solid squares indicate the optimal buffer sizes for each study area, as shown in Supplement Table 1.

3.3 Sensitivity of N_d to AOD

Eq. (2) shows that the value of the sensitivity of N_d to AOD is determined by the slope of a linear fit to a log-log plot of N_d versus AOD. To investigate S_{Nd}, we used correlated data pairs for each of the 7 years during periods 1 and 2, binned the data in AOD intervals with a bin width of 0.02, and the N_d data in each AOD bin were averaged. The variation of S_{Nd} with buffer size for different study areas over the target region is presented in Figure 8, for both periods. The data in Figure 8 show that, in contrast to S_{CER}, S_{Nd} is predominantly positive ($p<0.01$) during both periods, and decreases with increasing buffer size, except for the smallest study area during Period 1 and for spatial extends up to 30 km in period 2, when S_{Nd} may initially increase or vary. During Period 1, for the study area of 6°×6°, the S_{Nd} initially decreases very fast to a minimum at a buffer size of 40 to 50 km, followed by an increase to a maximum at a buffer size of 120 km. For buffer size ≥ 120 km, the S_{Nd} values are similar for the two smallest study areas and substantially larger than for the two larger study areas. During period 2, we can see an initial increase of S_{Nd} for the study area of 6°×6° and 8°×8°, and variation of S_{Nd} for the study area of 10°×10° and 4°×4°.

https://doi.org/10.5194/egusphere-2025-3157
Preprint. Discussion started: 10 October 2025

After that, the S_{Nd} for the study area of 4°×4° and 6°×6° decreases very fast to a minimum for a buffer size of 80 km, followed by an increase to maximum for a buffer size of 140 km. The variation of R with buffer size for each of the two periods shows that the optimal buffer sizes are larger when the study area is larger, i.e., in study areas of 8°×8° and 10°×10° they are larger than in smaller study area, i.e., 4°×4° and 6°×6° (Figure 9), reflecting different characteristics in aerosol-cloud interactions in different AOD conditions. The estimates of S_{Nd} and correlation coefficients R between N_d and AOD, stratified by optimal buffer size, for study areas ranging from 4°×4° to 10°×10° during the 2015–2022 period are presented in A2.

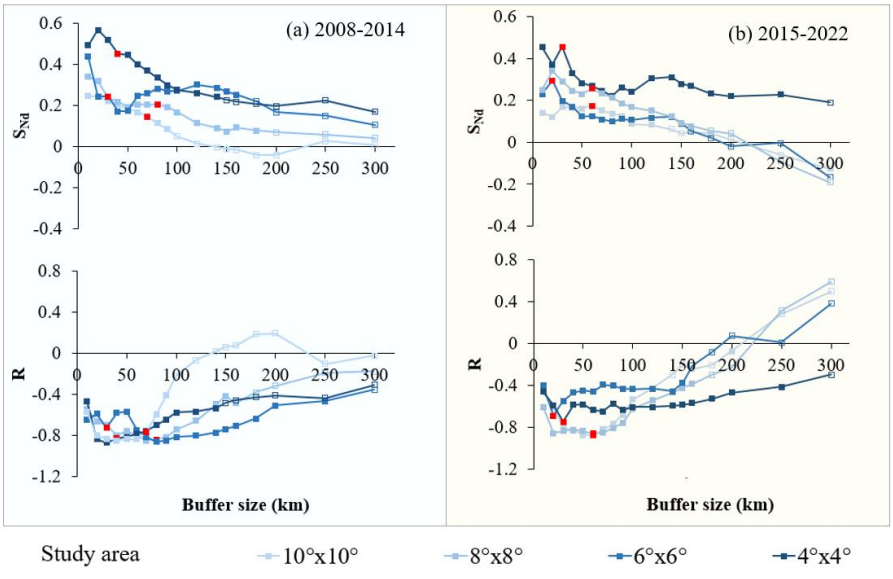

Figure 8. Variation of S_{Nd} (top) and correlation coefficient R (bottom) with buffer size for different study areas (see legend below the figures) for the LWP regime with 0<LWP≤200 g/m² over the years of 2008-2014 (a) and 2015-2022 (b). The solid square indicates that the results are significant at the 0.01 level and the hollow square indicates that the results are not statistically significant. The red solid square indicates the optimal buffer size for each study area, as shown in Supplement Table 2.

https://doi.org/10.5194/egusphere-2025-3157
Preprint. Discussion started: 10 October 2025

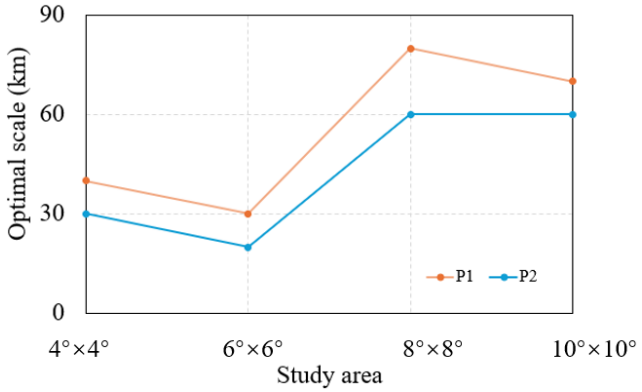

Figure 9. Relationship between optimal scale for N_d and the size of the study area. Here P1 and P2 indicate the optimal scale in period 2008-2014 and the optimal scale in period 2015-2022, respectively.

4 Discussion

4.1 The Importance of LWP constraint

LWP is a critical parameter governing cloud radiative properties (Murray-Watson et al., 2022). The quantification of albedo effects strongly depends on the spatial scale and the LWP. Neglecting LWP constraints in aerosol-cloud interaction studies can weaken microphysical signals, leading to underestimation of radiative forcing (McComiskey et al., 2012). To address this, we first systematically investigated the dynamic relationship between CER and LWP before analyzing CER sensitivity to AOD. The results demonstrate pronounced CER sensitivity to LWP variations, which can be categorized into three distinct phases:

At small LWP regime, CER increases rapidly with LWP, where CER evolution is predominantly driven by LWP changes. This dominance may lead to overestimation of the influence of the AOD on CER (Liu et al., 2021).

At intermediate LWP regime, CER decreases with increasing LWP. During this regime, the regulatory effect of LWP on CER weakens significantly, and CER variations become increasingly governed by aerosol-related processes, indicating the growing dominance of aerosol indirect effects.

The third regime contains an insufficient number of CER observations to yield statistically significant results, excluding analysis of the sensitivity of CER to AOD during this regime.

Comparative analysis of scale-conditioned S_{CER} across LWP regimes in periods 1 and 2 revealed

https://doi.org/10.5194/egusphere-2025-3157
Preprint. Discussion started: 10 October 2025

markedly enhanced sensitivity of S_{CER} to AOD during LWP regime 2. There is a trade-off between AOD and LWP when the amount of water vapor is insufficient and CER becomes smaller. As suggested by Costantino et al. (2013), the LWP response to aerosol invigoration is influenced by two competing mechanisms: a drying effect caused by enhanced entrainment of dry air at cloud top (dominant in optically thin clouds) and a moistening effect from precipitation suppression (dominant in optically thick clouds). When LWP is larger, the supply of cloud water is sufficient, and the increase in aerosol number concentrations significantly affects the distribution of cloud droplet number concentrations and sizes, enhancing the sensitivity of CER to AOD.

The smaller S_{CER} in the larger scale indicates that S_{CER} becomes smaller may be due to meteorological confounding effects. In addition, clouds with larger LWP are usually associated with strong updrafts (such as convective clouds), and stronger turbulence and vertical transport will bring more aerosols into the clouds, increasing CCN concentration and a decrease in particle size, making them more sensitive to changes in AOD. Therefore, this phenomenon is the result of the combined action of cloud microphysical processes (CCN activation, cloud droplet competition growth) and dynamic processes (updrafts, turbulent mixing). If the characteristics of aerosols in the second LWP regime (such as composition) change, this sensitivity may be further amplified. Consequently, the LWP-stratified S_{CER} quantification framework enables precise characterization of scale-dependent aerosol-cloud interactions, providing robust physical insights for climate effect assessments and effectively reducing uncertainties in future climate projections.

4.2 Scale effect of sensitivity of cloud parameters to aerosol variations

Extensive studies have demonstrated significant spatial scale dependence in aerosol indirect effect (McComiskey et al., 2012; Possner et al., 2016; Glotfelty et al., 2020; Ekman et al., 2023). Failure to explicitly define the scale-dependent behavior of aerosol indirect effect may introduce systematic biases and inconsistencies in subsequent process analyses. Based on satellite observations, this study confirms statistically significant negative correlations between CER and AOD, as well as positive correlations between N_d and AOD during both periods, aligning with classical aerosol-cloud interaction theory (Quaas et al., 2009). Analysis of scale-conditioned S_{CER} and S_{Nd} reveals that for fixed buffer size, an increase in the size of the study area leads to a systematic reduction in S_{CER} (less negative) and S_{Nd}, corroborating

https://doi.org/10.5194/egusphere-2025-3157
Preprint. Discussion started: 10 October 2025

the nonlinear attenuation of aerosol signals with spatial domain expansion (Quaas et al., 2009). The study verifies that AOD-cloud property correlations at large study areas are susceptible to meteorological confounding effects (Quaas et al., 2010; Boucher and Quaas, 2012; Gryspeerdt et al., 2014; Liu et al., 2024). This scale-dependent confounding mechanism elucidates uncertainties in aerosol indirect effect assessments at regional scales.

Multi-scale spatial analysis identifies different optimal buffer sizes for S_{CER} and S_{Nd} in different periods. These findings align closely with satellite-based aerosol indirect effect studies (Wang et al., 2015; Liu et al., 2017), providing critical scale benchmarks for satellite product validation. Wang et al. (2015) revealed an inverse "Twomey" effect between aerosols and CER in eastern China by analyzing aerosol and CER within a 50 km buffer zone around CALIOP samples. Similarly, Liu et al. (2017) systematically examined the response mechanisms of warm cloud macro- and microphysical parameters to increasing AOD in the Yangtze River Delta region, also using CALIOP samples within a 50 km buffer zone. The study further reveals that under decreasing aerosol concentrations, S_{CER} values across different study areas at the same buffer size exhibit convergence characteristics, with generally smaller S_{CER} (closer to zero). This indicates a significant weakening of aerosol-cloud interaction intensity and reduced spatial extent dependency under low aerosol loading conditions. Notably, these findings mechanistically align with the conclusion of Ma et al. (2015) that spatially aggregated pollutant emissions at higher resolutions amplify aerosol effects, demonstrating a nonlinear coupling between the spatial-resolution dependency of aerosol effects and their concentration gradients.

By systematically quantifying the scale-response characteristics of aerosol indirect effects, this work not only elucidates the dynamic scale behavior of aerosol-cloud interactions but, more critically, establishes criteria for determining optimal buffer size in regional aerosol indirect effect studies. Such advancements provide actionable insights for refining parameterization schemes in climate models, thereby enhancing their predictive reliability.

4.3 Limitations and implications

This study has three significant limitations. Firstly, similar to most previous studies (Wang et al., 2015; Liu et al., 2021), this study only utilized MODIS data with a resolution of 10 km to explore scale effects, ignoring finer or coarser resolution data. Therefore, using a 10 km buffer size as the minimum

https://doi.org/10.5194/egusphere-2025-3157
Preprint. Discussion started: 10 October 2025

observation unit, this limitation makes the indirect effects of aerosols on smaller scales still unknown, which may lead to inaccurate evaluation of aerosol indirect effects. Therefore, future research can improve the sensitivity of aerosol indirect effects to scale changes by using observation data with higher accuracy or model simulations. Secondly, the current research focuses on the influence of buffer size and study areas, the potential impact of spatial aggregation methods (especially zoning directionality) on the quantitative results of aerosol indirect effects has not been systematically evaluated. Future research should further investigate the sensitivity of aerosol indirect effects to zoning direction. Moreover, the current study employs a uniform buffer size for both aerosol and cloud parameters, failing to account for potential interaction effects arising from discrepancies of buffer size between them. Therefore, clarifying scale dependence will avoid directly extrapolating local observation results to a larger study area when downscaling climate models or formulating regional environmental policies.

5 Conclusions

Based on MODIS and CALIPSO satellite observations of aerosol and cloud parameters over land in eastern China, this study conducted a comparative analysis of the sensitivity of cloud microphysical parameters (CER and N_d) to variations in AOD during two characteristic periods: period 1 (2008-2014) and period 2 (2015-2022). Through systematic analysis of the relationship between CER and LWP and their response mechanisms to AOD across these two periods, the following key conclusions were drawn: Firstly, CER exhibited three distinct phases with varying LWP. During the rapid growth regime (LWP < 55/50 g/m²), CER showed significant negative sensitivity to AOD (S_{CER}), consistent with the Twomey effect; during the declining regime (LWP = 55-135/50-100 g/m²), S_{CER} remained negative but with enhanced sensitivity; and during the slow growth regime (LWP > 135/100 g/m²), the rate of CER change significantly decreased. These findings confirm that LWP is a crucial regulatory factor influencing the CER response to AOD.

Secondly, scale dependence analysis revealed significant scale-dependent characteristics in aerosol-cloud interaction. The results of the study show that S_{CER} systematically decreases as buffer size increases and becomes negligible for buffer sizes larger than 150-200 km, while the optimal buffer sizes vary substantially with the size of the study area in the range from 6°×6° to 10°×10°: increasing as study area increases during period 2, but decreasing in period 1 for regime 2. Particularly noteworthy is the enhanced

https://doi.org/10.5194/egusphere-2025-3157
Preprint. Discussion started: 10 October 2025

consistency of S_{CER} across different study areas and the significantly decreased S_{CER} during period 2, reflecting weaker aerosol-cloud interactions due to declining regional aerosol concentrations. Finally, the sensitivity of N_d to AOD (S_{Nd}) exhibited distinct characteristics compared to S_{CER}: S_{Nd} showed a significant positive correlation ($p < 0.01$) and demonstrated nonlinear attenuation with increasing buffer size and study area. The optimal buffer size for S_{Nd} was smaller during period 2 than during period 1 and increases with the study area size, being substantially larger for study areas of 8°×8° and 10°×10° than for study areas of 4°×4° and 6°×6° areas. These findings not only deepen our understanding of aerosol indirect effects but also provide important observational basis for improving aerosol-cloud parameterization schemes in climate models. The results emphasize that both the phased characteristics of LWP and spatial scale effects must be considered when assessing aerosol indirect effect.

Data availability

All data used in this study are publicly available. The satellite data from the MODIS instrument used in this study were obtained from https://ladsweb.nascom.nasa.gov/search/ (last access: 02 July 2025). The satellite data from CALIOP were obtained from https://subset.larc.nasa.gov/calipso/login.php (last access: 02 July 2025).

Author contributions

YL, LT and GL designed the research. YL and LT led the analyses. YL and GL wrote the manuscript with major input from JH, and further input from all other authors. All authors contributed to interpreting the results and to the finalization and revision of the manuscript.

Competing interests

The authors declare that they have no conflict of interest.

Acknowledgements

The authors greatly appreciate NASA CloudSat Data Processing Center that provided the data used in this study. This work was supported by the National Natural Science Foundation of China (Grant No. 42001290), the Natural Natural Science Foundation of China (Grant No. 42271299), and the Natural

https://doi.org/10.5194/egusphere-2025-3157
Preprint. Discussion started: 10 October 2025

Science Foundation Project of Xiamen (Grant No. 3502Z202472037). Gerrit de Leeuw is supported by the Chinese Academy of Sciences President's International Fellowship Initiative. Grant No. 2025PVA0014.

References

Albrecht, B. A.: Aerosols, cloud microphysics, and fractional cloudiness, Science, 245, 1227-1230, 1989.

Bellouin, N., Quaas, J., Gryspeerdt, E., Kinne, S., Stier, P., Watson-Parris, D., et al.: Bounding global aerosol radiative forcing of climate change. Reviews of Geophysics, 58, e2019RG000660. https://doi.org/10. 1029/2019RG000660, 2020.

Altaratz, O., Koren, I., Remer, L.A., Hirsch, E.: Review: Cloud invigoration by aerosols—Coupling between microphysics and dynamics. Atmospheric Research, 140-141, 38-60, 2014.

Andreae, M. O.: Correlation between cloud condensation nuclei concentration and aerosol optical thickness in remote and polluted regions, Atmos. Chem. Phys., 9, 543-556, https://doi.org/10.5194/acp-9-543-2009, 2009.

Bender, F.A.M., Frey, L., McCoy, D.T., Grosvenor, D.P., Mohrmann, J.K.: Assessment of aerosol–cloud–radiation correlations in satellite observations, climate models and reanalysis. Climate Dynamics, 52, 4371-4392, 2019.

Boucher, O., Quaas, J.: Water vapour affects both rain and aerosol optical depth. Nature Geoscience, 6(1), 4-5. https://doi.org/10.1038/ngeo1692, 2012.

Bréon, F. M., Tanré, D., Generoso, S.: Aerosol effect on cloud droplet size monitored from satellite, Science, 295(5556):834-8. doi: 10.1126/science.1066434, 2002.

Bulgin, C. E., Palmer, P.I., Thomas, G.E., Arnold, C.P.G., Campmany, E., Carboni, E., Grainger, R. G., Poulsen, C., Siddans, R., Lawrence, B.N.: Regional and seasonal variations of the Twomey indirect effect as observed by the ATSR-2 satellite instrument, Geophysical Research Letters, 35, 2, 2008.

Chen, G., W.-C.Wang, and J.-P. Chen, 2015: Aerosol–stratocumulus–radiation interactions over southeast Pacific. J. Atmos. Sci., 72, 2612–2621, https://doi.org/10.1175/JAS-D-14-0319.1.

https://doi.org/10.5194/egusphere-2025-3157
Preprint. Discussion started: 10 October 2025

Chen, Y.-C., Christensen, M. W., Stephens, G. L., and Seinfeld, J. H.: Satellite-based estimate of global aerosol-cloud radiative forcing by marine warm clouds, Nat. Geosci., 7, 643–646, https://doi.org/10.1038/ngeo2214, 2014.

Christensen, M. W., Chen, Y.-C., and Stephens, G. L.: Aerosol indirect effect dictated by liquid clouds, J. Geophys. Res., 121, 14636-14650, https://doi.org/10.1002/2016JD025245, 2016.

Costantino, L. and Bréon, F. M.: Analysis of aerosol-cloud interaction from multi-sensor satellite observations. Geophys. Res. Lett., 37, L11801, doi:10.1029/2009GL041828, 2010.

Costantino, L. and Bréon, F. M.: Aerosol indirect effect on warm clouds over South-East Atlantic, from co-located MODIS and CALIPSO observations, Atmos. Chem. Phys., 13: 69-88, 2013.

de Leeuw, G., R. van der A, J. Bai, Y. Xue, C. Varotsos, Z. Li, C. Fan, X. Chen, I. Christodoulakis, J. Ding, X. Hou, G. Kouremadas, D. Li, J. Wang, M. Zara, K. Zhang, Y. Zhang.: Air Quality over China. Remote Sens. 2021, 13, 3542. https://doi.org/ 10.3390/rs13173542, 2021.

de Leeuw, G., Fan, C, Li, Z., Dong, J., Li, Y., Ou, Y., and Zhu, S. (2022). Spatiotemporal variation and provincial scale differences of the AOD across China during 2000–2021. Atmospheric Pollution Research 13 (2022) 101359 (14 pp). https://doi.org/10.1016/j.apr.2022.101359.

de Leeuw, G., Kang, H., Fan, C., Li, Z., Fang, C., Zhang, Y. (2023). Meteorological and anthropogenic contributions to changes in the Aerosol Optical Depth (AOD) over China during the last decade. Atm. Env., 301, 119676. https://doi.org/10.1016/j.atmosenv.2023.119676.

Ekman, A. M. L., Eva Nygren, Alejandro Baró Pérez, Matthias Schwarz, Gunilla Svensson, Nicolas Bellouin.: Influence of horizontal resolution and complexity of aerosol–cloud interactions on marine stratocumulus and stratocumulus-to-cumulus transition in HadGEM3-GC3.1, Quart. J Royal Met Soc., 149, 755, 2049-2066, https://doi.org/10.1002/qj.4494, 2023.

Fan J, Wang Y, Rosenfeld D, et al.: Review of aerosol-cloud interactions: Mechanisms, significance, and challenges. Journal of the Atmospheric Sciences,73(11): 4221-4252, 2016.

Feingold, G., Remer, L. A., Ramaprasad, J., Kaufman, Y. J.: Analysis of smoke impact on clouds in Brazilian biomass burning regions: an extension of Twomey's approach, J. Geophys. Res., 106 (D19), 22907-22922, 2001.

Feingold, G., Goren, T., and Yamaguchi, T.: Quantifying albedo susceptibility biases in shallow clouds, Atmos. Chem. Phys., 22, 3303–3319, https://doi.org/10.5194/acp-22-3303-2022, 2022.

https://doi.org/10.5194/egusphere-2025-3157
Preprint. Discussion started: 10 October 2025

605 Grandey, B.S., Stier, P.: A critical look at spatial scale choices in satellite-based aerosol indirect effect
606 studies. Atmos. Chem. Phys., 10, 11459-11470, 2010.
607 Gryspeerdt, E., Stier, P., and Partridge, D. G.: Satellite observations of cloud regime development: the
608 role of aerosol processes, Atmos. Chem. Phys., 14, 1141-1158, doi:10.5194/acp-14-1141-2014, 2014.
609 Gryspeerdt, E., Povey, A. C., Grainger, R. G., Hasekamp, O., Hsu, N. C., Mulcahy, J. P., Sayer, A. M.,
610 and Sorooshian, A.: Uncertainty in aerosol–cloud radiative forcing is driven by clean conditions, Atmos.
611 Chem. Phys., 23, 4115-4122, https://doi.org/10.5194/acp-23-4115-2023, 2023.
612 Gryspeerdt, E., McCoy, D. T., Crosbie, E., Moore, R. H., Nott, G. J., Painemal, D., Small-Griswold, J.,
613 Sorooshian, A., and Ziemba, L.: The impact of sampling strategy on the cloud droplet number
614 concentration estimated from satellite data, Atmos. Meas. Tech., 15, 3875–3892, 2022,
615 https://doi.org/10.5194/amt-15-3875-2022, 2022.
616 Glotfelty, T., Kiran Alapaty, Jian He, Patrick Hawbecker, Xiaoliang Song, and Guang Zhang. Studying
617 Scale Dependency of Aerosol–Cloud Interactions Using Multiscale Cloud Formulations, 77, 11, 2020.
618 Grosvenor, D. P., Sourdeval, O., Zuidema, P., Ackerman, A., Alexandrov, M. D., Bennartz, R., Boers,
619 R., Cairns, B., Chiu, J. C., Christensen, M., Deneke, H., Diamond, M., Feingold, G., Fridlind, A.,
620 Hünerbein, A., Knist, C., Kollias, P., Marshak, A., McCoy, D., Merk, D., Painemal, D., Rausch, J.,
621 Rosenfeld, D., Russchenberg, H., Seifert, P., Sinclair, K., Stier, P., Diedenhoven, B. V., Wendisch, M.,
622 Werner, F., Wood, R., Zhang, Z., and Quaas, J.: Remote sensing of droplet number concentration in
623 warm clouds: A review of the current state of knowledge and perspectives, Rev. Geophys., 56, 409–453,
624 https://doi.org/10.1029/2017RG000593, 2018.
625 Jia, H. L., Ma, X. Y., Quaas, J., Yin, Y., Qiu, T.: Is positive correlation between cloud droplet effective
626 radius and aerosol optical depth over land due to retrieval artifacts or real physical processes?
627 Atmospheric Chemistry and Physics, 19, 13, 8879-8896, 2019.
628 Jones, T. A., Christopher, S. A., & Quaas, J.: A six year satellite-based assessment of the regional
629 variations in aerosol indirect effects. Atmospheric Chemistry and Physics, 9, 4091, 2009.
630 Koren, I., Kaufman, Y. J., Rosenfeld, D., Remer, L. A., Rudich, Y.: Aerosol invigoration and
631 restructuring of Atlantic convective clouds. Geophys. Res. Lett., 32 (14), L14828, 2005.
632 Kaufman, Y.J. and Fraser, R.S.: The effect of smoke particles on clouds and climate forcing. Science,
633 1997. 277(5332): p. 1636-1639.

https://doi.org/10.5194/egusphere-2025-3157
Preprint. Discussion started: 10 October 2025

Kaufman, Y.J., Remer, L.A., Tanré, D., Li, R.R., Kleidman, R., Mattoo, S., Levy, R.C., Eck, T.F., Holben, B.N., Ichoku, C., Member, IEEE, Martins, J.V., and Koren, I.: A Critical Examination of the Residual Cloud Contamination and Diurnal Sampling Effects on MODIS Estimates of Aerosol Over Ocean, IEEE TRANSACTIONS ON GEOSCIENCE AND REMOTE SENSING, 43, 12, 2005.

Kim, S. W., S. C. Yoon, J. Y. Kim, and S. Y. Kim (2007), Seasonal and monthly variations of columnar aerosol optical properties over East Asia determined from multi-year MODIS, LIDAR, and AERONET Sun/sky radiometer measurements, Atmos. Environ., 41(8), 1634–1651, doi:10.1016/j.atmosenv.2006.10.044.

King, M. D., Tsay, S. C., Platnick, S. E., Wang, M., and Liou, K. N.: Cloud Retrieval Algorithms for MODIS: Optical Thickness, Effective Particle Radius, and Thermodynamic Phase, MODIS Algorithm Theoretical Basis Document, available at: http://eospso.nasa.gov/sites/default/files/atbd/atbd_mod05.pdf, 1997.

King, M. D., Menzel, W. P., Kaufman, Y. J., Tanré, D., Gao, B. C., Platnick, S., Ackerman, S. A., Remer, L. A., Pincus, R., and Hubanks, P. A.: Cloud and aerosol properties, precipitable water, and profiles of temperature and water vapor from MODIS, IEEE T. Geosci. Remote, 41, 442–458, doi:10.1109/TGRS.2002.808226, 2003.

Lebsock, M., Morrison, H., Gettelman, A.: Microphysical implications of cloud-precipitation covariance derived from satellite remote sensing. Journal of Geophysical Research: Atmosphere, 118, 6521-6533, 2013.

Levy, R. C., Remer, L. A., Kleidman, R. G., Mattoo, S., Ichoku, C., Kahn, R., and Eck, T. F.: Global evaluation of the Collection 5 MODIS dark-target aerosol products over land, Atmos. Chem. Phys., 10, 10399–10420, doi:10.5194/acp-10-10399-2010, 2010.

Liu, Y., Lin, T., Zhang, J., Wang, F., Huang, Y., Wu, X., Ye, H., Zhang, G., Cao, X., and de Leeuw, G.: Opposite effects of aerosols and meteorological parameters on warm clouds in two contrasting regions over eastern China, Atmos. Chem. Phys., 24, 4651–4673, https://doi.org/10.5194/acp-24-4651-2024, 2024.

Liu, Q., Duan, S. Y., He, Q. S., Chen, Y. H., Zhang, H., Cheng, N. X., Huang, Y. W., Chen, B., Zhan, Q. Y., Li, J. Z.: The variability of warm cloud droplet radius induced by aerosols and water vapor in Shanghai from MODIS observations, Atmospheric Research, 253, 105470, 2021.

https://doi.org/10.5194/egusphere-2025-3157
Preprint. Discussion started: 10 October 2025

Liu, T. Q., Liu, Q., Chen, Y. H., Wang, W. C., Zhang, H., Li, D., Sheng, J.: Effect of aerosols on the macro- and micro-physical properties of warm clouds in the Beijing-Tianjin-Heibei region. Science of the Total Environmen, 720, 137618, 2020.

Liu, Y., Zhang, J., Zhou, P., Lin, T., Hong, J., Shi, L., Yao, F., Wu, J., Guo, H., and de Leeuw, G.: Satellite-based estimate of the variability of warm cloud properties associated with aerosol and meteorological conditions, Atmos. Chem. Phys., 18, 18187-18202, https://doi.org/10.5194/acp-18-18187-2018, 2018.

Liu, Y., de Leeuw, G., Kerminen, V.-M., Zhang, J., Zhou, P., Nie, W., Qi, X., Hong, J., Wang, Y., Ding, A., Guo, H., Krüger, O., Kulmala, M., and Petäjä, T.: Analysis of aerosol effects on warm clouds over the Yangtze River Delta from multi-sensor satellite observations, Atmos. Chem. Phys., 17, 5623-5641, https://doi.org/10.5194/acp-17-5623-2017, 2017.

Liu, Z., Vaughan, M., Winker, D., Kittaka, C., Getzewich, B., Kuehn, R., Omar, A.,Powell, K., Trepte, C., and Hostetler, C.:The CALIPSO lidar cloud and aerosol discrimination: Version 2 algorithm and initial assessment of performance, J. Atmos. Ocean. Tech., 26, 1198–1213, 2009.

Ma, X., Jia, H., Yu, F., and Quaas, J.: Opposite aerosol index-cloud droplet effective radius correlations over major industrial regions and their adjacent oceans, Geophys. Res. Lett., 45, 5771–5778, https://doi.org/10.1029/2018GL077562, 2018.

Ma, P.-L., P. J. Rasch, M. Wang, H. Wang, S. J. Ghan, R. C. Easter, W. I. Gustafson Jr., X. Liu, Y. Zhang, and H.-Y. Ma (2015), How does increasing horizontal resolution in a global climate model improve the simulation of aerosol-cloud interactions?, Geophys. Res. Lett., 42, 5058–5065, doi:10.1002/2015GL064183.

Matheson, M. A., Coakley Jr., J. A., and Tahnk, W. R.: Aerosol and cloud property from relationships for summer stratiform clouds in the northeastern Atlantic from advanced very high resolution radiometer observations, J. Geophys. Res., 110, D24204, doi:10.1029/2005JD006165, 2005.

McComiskey, A., & Feingold, G: The scale problem in quantifying aerosol indirect effects. Atmospheric Chemistry and Physics, 12, 1031. https://doi.org/10.5194/acp-12-1031-2012, 2012.

Meskhidze, N., Nenes, A.: Effects of ocean ecosystem on marine aerosol-cloud interaction. Adv. Meteorol, doi:10.1155/2010/239808, 2010.

https://doi.org/10.5194/egusphere-2025-3157
Preprint. Discussion started: 10 October 2025

691 Murray-Watson, R. J. and Gryspeerdt, E.: Stability-dependent increases in liquid water with droplet
692 number in the Arctic, Atmos. Chem. Phys., 22, 5743–5756, https://doi.org/10.5194/acp-22-5743-2022,
693 2022.
694 McComiskey, A., G. Feingold, A. S. Frisch, D. D. Turner, M. A. Miller, J. C. Chiu, Q. Min, and J. A.
695 Ogren (2009), Anassessment of aerosol-cloud interactions in marine stratus clouds based on surface
696 remote sensing, J. Geophys. Res., 114, D09203,doi:10.1029/2008JD011006.
697 Possner A., E. M. Zubler, U. Lohmann, and C. Schär (2016), The resolution dependence of cloud effects
698 and ship-induced aerosol-cloud interactions in marine stratocumulus, J. Geophys. Res. Atmos., 121,
699 4810–4829, doi:10.1002/2015JD024685.
700 Pandey, S. K., Vinoj, V., Panwar, A.: The short-term variability of aerosols and their impact on cloud
701 properties and radiative effect over the Indo-Gangetic Plain. Atmospheric Pollution Research, 11, 630-
702 638, 2020.
703 Platnick, S., Meyer, K. G., King, M. D., Wind, G., Amarasinghe, N., Marchant, B., Arnold, G. T., Zhang,
704 Z., Hubanks, P. A., Holz, R. E., Yang, P., Ridgway, W. L., Riedi, J.: The MODIS cloud optical and
705 microphysical products: Collection 6 updates and examples from Terra and Aqua. IEEE Trans Geosci
706 Remote Sens. Jan;55(1):502-525. doi: 10.1109/TGRS.2016.2610522, 2017.
707 Quaas, J., Boucher, O., Bellouin, N., Kinne, S.: Satellite-based estimate of the direct and indirect aerosol
708 climate forcing, J. Geophys. Res., 113, D05204, doi:10.1029/2007JD008962, 2008.
709 Quaas, J., Stevens, B., Stier, P., and Lohmann, U.: Interpreting the cloud cover – aerosol optical depth
710 relationship found in satellite data using a general circulation model, Atmos. Chem. Phys., 10, 6129-
711 6135, https://doi.org/10.5194/acp-10-6129-2010, 2010.
712 Quaas, J., Boucher, O., and Lohmann, U.: Constraining the total aerosol indirect effect in the LMDZ and
713 ECHAM4 GCMs using MODIS satellite data, Atmos. Chem. Phys., 6, 947–955,
714 https://doi.org/10.5194/acp-6-947-2006, 2006.
715 Quaas, J., Ming, Y., Menon, S., Takemura, T., Wang, M., Penner, J. E., Gettelman, A., Lohmann, U.,
716 Bellouin, N., Boucher, O., Sayer, A. M., Thomas, G. E., McComiskey, A., Feingold, G., Hoose, C.,
717 Kristjánsson, J. E., Liu, X., Balkanski, Y., Donner, L. J., Ginoux, P. A., Stier, P., Grandey, B., Feichter,
718 J., Sednev, I., Bauer, S. E., Koch, D., Grainger, R. G., Kirkevåg, A., Iversen, T., Seland, Ø., Easter, R.,
719 Ghan, S. J., Rasch, P. J., Morrison, H., Lamarque, J.-F., Iacono, M. J., Kinne, S., and Schulz, M.: Aerosol

https://doi.org/10.5194/egusphere-2025-3157
Preprint. Discussion started: 10 October 2025

indirect effects – general circulation model intercomparison and evaluation with satellite data, Atmos. Chem. Phys., 9, 8697–8717, https://doi.org/10.5194/acp-9-8697-2009, 2009.

Rao, S., Dey, S.: Consistent signal of aerosol indirect and semi-direct effect on water clouds in the oceanic regions adjacent to the Indian subcontinent. Atmospheric Research, 232, 2020.

Remer, L. A., Kaufman, Y. J., Tanre, D., Mattoo, S., Chu, D. A., Martins, J. V., Li, R. R., Ichoku, C., Levy, R. C., Kleidman, R. G., Eck, T. F., Vermote, E., and Holben, B. N.: The MODIS aerosol algorithm, products, and validation, J. Atmos. Sci., 62, 947–973, https://doi.org/10.1175/JAS3385.1, 2005.

Rosenfeld, D., Zhu, Y. N., Wang, M. H., Zheng, Y. T., Goren, T., Yu, S. C.: Aerosol-driven droplet concentrations dominate coverage and water of oceanic low-level clouds, Science, 363, 6427, 2019.

Saponaro, G., Kolmonen, P., Sogacheva, L., Rodriguez, E., Virtanen, T., de Leeus, G.: Estimates of the aerosol indirect effect over the Baltic Sea region derived from 12 years of MODIS observations, Atmos. Chem. Phys., 17, 3133-3143, 2017.

Stephens, G., Vane, D. G., Boain, R. J., Mace, G. G., Sassen, K., Wang, Z., Illingworth, A. J., O'Connor, E. J., Rossow, W. B., Durden, S. L., Miller, S. D., Austin, R. T., Benedetti, A., and Mitrescu, C.: The CloudSat Science Team: The CloudSat mission and the A-Train, B. Am. Meteorol. Soc., 83, 1771–1790, 2002.

Sourdeval, O., Laurent C.-Labonnote, Anthony J. Baran, Johannes Mülmenstädt, Gérard Brogniez.: A methodology for simultaneous retrieval of ice and liquid water cloud properties. Part 2: Near-global retrievals and evaluation against A-Train products, Quarterly Journal of the Royal Meteorological Society, 142, 701, 3063-3081, 2016.

Sundström, A.-M., Kolmonen, P., Sogacheva, L., and de Leeuw, D.: Aerosol retrievals over China with the AATSR dual view algorithm, Remote Sens. Environ., 116, 189–198, 2012.

Theodore L. Anderson, Robert J. Charlson, David M. Winker, John A. Ogren, and Kim Holmén.: Mesoscale Variations of Tropospheric Aerosols, Journal of the Atmospheric Sciences, 60, 1, https://doi.org/10.1175/1520-0469(2003)060<0119:MVOTA>2.0.CO;2, 2003.

Tang, J., Wang, P., Mickley, L. J., Xia, X., Liao, H., Yue, X., et al.: Positive relationship between liquid cloud droplet effective radius and aerosol optical depth over Eastern China from satellite data. Atmospheric Environment, 84, 244-253. https://doi.org/10.1016/j.atmosenv.2013.08.024, 2014.

https://doi.org/10.5194/egusphere-2025-3157
Preprint. Discussion started: 10 October 2025

Tao, W. K., Chen, J. P., Li, Z., Wang, C. E., Zhang, C. D.: Impact of aerosols on convective clouds and precipitation, Reviews of Geophysics, 50(2), 2012.

Twomey, S.: The influence of pollution on the shortwave albedo of clouds, J. Atmos. Sci. 34(7), 1149-1152, 1977.

Wang, F., Guo, J., Zhang, J., Wu, Y., Zhang, X., Deng, M., and Li, X.: Satellite observed aerosol-induced variability in warm cloud properties under different meteorological conditions over eastern China, Atmos. Environ., 84, 122–132, 2014.

Wang, F., Guo, J., Zhang, J., Wu, Y., Zhang, X., Deng, M., Li, X.: Satellite observed aerosol-induced variability in warm cloud properties under different meteorological conditions over eastern China, Atmos. Environ., 84, 122-132, 2014.

Winker, D. M., Pelon, J. R., and McCormick, M. P.: The CALIPSO mission: Spacebornelidar for observation of aerosols and clouds, Proc. SPIE, Lidar Remote Sensing for Industry and Environment Monitoring III, 4893, doi:10.1117/12.466539, 2003.

Wang, F., Guo, J., Zhang, J., Huang, J., Min, M., Chen, T., Liu, H., Deng, M., Li, X.: Multi-sensor quantification of aerosol-induced variability in warm clouds over eastern China, Atmos. Environ., 113: 1-9, 2015. http://dx.doi.org/10.1016/j.atmosenv.2015.04.063.

Yuan, T., Li, Z., Zhang, R., and Fan, J.: Increase of cloud droplet size with aerosol optical depth: an observation and modeling study, J. Geophys. Res., 113, D04201, doi:10.1029/2007JD008632, 2008.

Appendices

A1. Estimates of S_{CER}, computed using Eq. (1), and correlation coefficients R between CER and AOD, stratified by LWP, and optimal buffer size (see text), for study areas varying from 4°×4° to 10°×10°, during the periods 2008-2014 and 2015-2022. Statistically significant data points are indicated with * (p value < 0.01).

Years	LWP（g/m^2）	Study area	Optimal scale (km)	S_{CER}	R
2008-2014	0-55	10°×10°	30	-0.0858	0.8828*
		8°×8°	40	-0.1026	0.9220*
		6°×6°	100	-0.1305	0.8939*
		4°×4°	50	-0.2232	0.8459*
	55-135	10°×10°	40	-0.1275	0.8377*
		8°×8°	60	-0.1587	0.8978*
		6°×6°	30	-0.2061	0.9245*
		4°×4°	50	-0.3189	0.9096*
2015-2022	0-50	10°×10°	80	-0.0885	0.9082*
		8°×8°	40	-0.1138	0.8886*

https://doi.org/10.5194/egusphere-2025-3157
Preprint. Discussion started: 10 October 2025

		6°×6°	20	-0.1517	0.7618*
		4°×4°	50	-0.0863	0.6403*
		10°×10°	100	-0.1084	0.8717*
		8°×8°	90	-0.1354	0.8910*
	50-100	6°×6°	60	-0.1514	0.8384*
		4°×4°	60	-0.2212	0.8318*

A2. Estimates of S_{Nd}, computed using Eq. (2), and correlation coefficients R between N_d and AOD, stratified by optimal buffer size (see text) for study areas varying from 4°×4° to 10°×10°, during the periods 2008-2014 and 2015-2022. Statistically significant data points are indicated with * (p value < 0.01).

Years	Study area	Optimal scale (km)	S_{Nd}	R
2008-2014	10°×10°	70	0.1434	-0.8507*
	8°×8°	80	0.2045	-0.8646*
	6°×6°	30	0.2430	-0.8741*
	4°×4°	40	0.4496	-0.8523*
2015-2022	10°×10°	60	0.1742	-0.8788*
	8°×8°	60	0.2682	-0.8638*
	6°×6°	20	0.2964	-0.6900*
	4°×4°	30	0.2903	-0.7478*